9

Boron Studies in Interdisciplinary Fields Employing Nuclear Track Detectors (NTDs)

László Sajo-Bohus[1], Eduardo D. Greaves[1] and József K. Pálfalvi[2]
[1]*Universidad Simón Bolívar, Valle de Sartenejas, Caracas,*
[2]*HAS KFKI Atomic Energy Research Institute, Budapest,*
[1]*Venezuela*
[2]*Hungary*

1. Introduction

The aims of this study is the dissemination of the major experimental results in applied fields involving the boron-10 neutron capture with emphasis on advances of interdisciplinary fields employing passive nuclear track techniques. The stable isotope boron-10 has found many applications in various fields of physics and other branches of science. In this study details on applications and methodology are given.

2. Elemental Boron nuclear properties

Boron is a natural element having two stable isotopes. ^{11}B (80.1%) and ^{10}B (19.9%). Only the latter has a high thermal neutron capture cross section (3832 b). Due to its nuclear characteristics e.g. being a non radioactive element and readily available, the isotope boron-10 is often employed in application where the (n, α) reaction is of advantage and where other analytical techniques could not be employed satisfactorily. The probability for absorption of a neutron by this stable isotope via the ^{10}B(n,α)^{7}Li capture reaction (^{10}BNC-reaction), is given by the absorption cross section. Its value is a function of the impinging neutron energy, (www.nndc.bnl.gov). The energetic fragments emitted in the ^{10}BNC-reaction produce a high value of "Linear Energy Transfer" (LET) or dE/dx, that is, a measure of the number of ionisations per unit distance as they traverse the absorbing material. Their combined path lengths are of short distance making them quite suitable where localized damage is of advantage. Industrial processes have been devised to modify the natural boron isotopic composition in order to obtain high values for ^{10}B concentration. Among the known boron compounds, several hundred are employed in today's applications and a growing list exists that enter the literature as related research progresses, Wikipedia (2011). Often natural boron is contained in biological material, in cells and it would be convenient to replace it with isotope enriched element. The possibility to introduce the ^{10}B isotope in any cell culture opened a new technique to treat e.g. cancer by Boron Neutron Capture Therapy (or ^{10}BNC Therapy). Chemical compounds containing^{10}B isotope are employed in purpose made specific applications such as neutron radiation shielding, nuclear reactors reactivity control, emergency shut-down systems, as occurred in the Fukushima No-1 nuclear power plant. Boron fibbers such as BN-nanotube material find the most convenient

application as structural material for spacecraft and radiation shielding. The ^{10}BNC-reaction to take place requires a sample containing, even at ppb level, ^{10}B, a source set for irradiation with thermal or lower neutron energy (0.025eV or less) and a reaction fragment detecting device. The reaction phenomenon is related to a neutron interacting with boron nucleus, followed by breakup in two fragment of the ^{10}B+n compound nucleus (that survives a short time in the order of picoseconds). The two fragment nuclei depart acquiring kinetic energy due to a strong Coulomb field moving in opposite direction under the momentum conservation law, synthesized by the following process:

$$\begin{array}{l} \qquad\qquad\qquad\quad {}^{7}\mathrm{Li} + {}^{4}\mathrm{He} + 2{,}79\ \mathrm{MeV}\ (\text{branching ratio } 6.1\%) \\ \qquad\qquad\qquad\quad \nearrow \\ {}^{10}\mathrm{B} + \mathrm{n} \dashrightarrow [\,{}^{11}\mathrm{B}] \qquad\qquad\qquad\qquad (1) \\ \qquad\qquad\qquad\quad \searrow \\ \qquad\qquad\qquad\quad {}^{7}\mathrm{Li} + {}^{4}\mathrm{He} + \gamma\ (0{,}48\ \mathrm{MeV}) + 2{,}31\ \mathrm{MeV}\ (\text{branching ratio } 93.9\ \%) \end{array}$$

The reaction occurs with different branching ratio: the first has a relatively low frequency occurrence (6.1%) but has the advantage that the reaction is photon less and therefore the induced damage leads to a higher "Linear Energy Transfer" (LET) or dE/dx. The other, with higher occurrence is accompanied by a 0,48 MeV photon. If the alpha particle (^{4}He^{+}) leave the sample surface, with sufficient kinetic energy, then it can be detected e.g. by nuclear track techniques. The alpha particle fingerprint given by a suitable detecting material, provides information on the boron presence and it is recognized as a powerful analytical method for boron studies.

3. Experimental set up

In general terms the experimental system consists of a neutron source with a collimator to obtain the required beam characteristics, radiation shielding, sample and detecting device. Often it is necessary to take into account diffusion effects due to neutron scattering taking place due to the geometry and location of moderating materials, either in a material external to the sample under scrutiny, or in the sample itself. Charged particles emitted by the ^{10}BNC-reaction have path lengths, in most absorbing material either a cell or a nuclear track detector (NTD), around 12 μm, being sufficient to induce large molecular damage.

3.1 Thermal and cold neutron beam production

Neutron irradiation is obtained by different systems in which thermal neutron flux is a prevailing component. The selection of the experimental arrangement depends mainly on the required beam intensity (e.g. for ^{10}BNC-therapy > 5x10^{8} ncm^{-2}s^{-1}) and its spectral characteristics (high % for thermal-epithermal fraction). Some aspects for selected application as well as sample size, geometry, chemical compound and density should be taken into account. If the application requires a high intensity beam, a major facility either a neutron reactor or an accelerator driven neutron source should be considered. However, for most applications it is sufficient to employ small, even portable, neutron generators (NG) or radioisotope neutron sources (RINS) offered commercially (QSA Global Inc., 40 North Avenue, Burlington, MA 01803). Some rather complex NG has been devised e.g. highly

compact fusion neutron source with a small sub-critical fission assembly to multiply the neutron source intensity. Leung et al. (2002) have patented a high current density NG employing coaxial RF-driven plasma ion source, particularly advantageous in medical applications since it provides a neutron flux of 1.2 x 10^{12} n/cm^2 s (by 2.4 MeV D-D reaction). Persaud et al., (2011) developed recently a new concept for ionizing deuterium atoms to obtain neutrons from the D-D reaction. Ingenious NG device developed by Naranjo, et al., (2005) envisioned a tabletop device suitable for many industrial applications. Other physical solutions have been adopted to obtain the thermal neutron beam and some expensive technical approaches are currently employed. For instance, to extend the RINS operational efficiency, liquid nitrogen is used to lower the thermal neutron energy. Another method to produce a pure thermal beam is to employ a neutron guide as available at the Budapest Neutron Centre (Budapest, Hungary, http://www.bnc.hu/). Primary neutron field, either from fission chain, nuclear reaction involving spallation, beam fragmentation or RINS, have an energy distribution from which suitable neutron beams in thermal region may be derived. This process requires some technical arrangement involving hydrogen or deuterium rich materials (heavy water, PVC and others) that reduce the energy spectrum to the required energy window (close or lower to the thermal neutron group). On the other hand due to restrictions imposed by scattering and other physics laws, it is difficult to obtain a pure thermal beam, even in the case of an accelerator produced monoenergetic beams. The most employed technique to select neutrons of a given energy group, is time of flight. Recently Stevenato et al. (2010), for non-destructive identification, developed a time-tagged ^{252}Cf source. Based on these techniques, the experimenter can take advantage to obtain the maximum ^{10}BNC-reaction yield.

4. Basic aspects of nuclear track techniques

4.1 Linear energy transfer and latent nuclear track formation

Solid state nuclear track detectors (SSNTD) or more briefly NTDs are capable to detect charged particles within certain circumstances. They can be natural crystals or special plastics. Their theory was developed more than 40 years ago, the basic fundamentals can be found in Somogyi (1973) and in more details in Durrani et al. (1987). Even more details for detecting alpha particles, which is important from BNCT point of view, can be found in Nikezic (2003). Therefore, here we touch some aspects of interest, only. Popularly saying, an ionizing particle produces a narrow damaged zone in the plastic, 10-100 nm in diameter, which can be enlarged and visualized by a chemical treatment, so that the particle movement in the detector material, let us say the footprint of the particle or its track can be followed under optical microscope. Depending on the chemical treatment (called etching) and observation method there are basically two requirements: the range and energy deposition of the particle should be adequate. For instance, if we apply a 6 N NaOH solution at 70 °C for 2 hours and an optical microscope, the range of the alpha particle should be at least 2.8 μm, which requires minimum 400 keV kinetic energy. In this case, the energy deposition, the linear energy transfer or LET, is quite enough, ~ 200 keV/μm, to provide enough damage to be visualized. The essence of the visualization is that the chemical removes the damaged material from the zone more quickly than the undamaged, bulk material, from the surfaces of the plastic. Two quantities are responsible for this process: the track etch velocity, V_T and the bulk etch velocity, V_B. Evidently, V_T should be > than V_B. The length and diameter of the track formed characterize the incident particle: its type and energy. These are what we need to know for studying the physical aspects of the boron study.

If we approach the alpha particle detection mechanism by the attitude of a physicist some more details should be given, as follow below.

Ionizing radiation may induce atomic or molecular modifications that are observed as structural defects in the absorber such as polyallyl-diglicol-carbonate, PADC or similar materials. In particular, energetic alpha particles through Coulomb interaction induce ionization and consequently provide high charge density to displace Atoms. Two kinds of processes are involved:

i. The impinging alpha particles, having energy above a value of ~100 keV, transfer their kinetic energy to electrons encountered on their path; this process is referred as Electronic Energy Loss, (Se),
ii. The energy is transferred directly to the atomic nucleus; in this case we have Nuclear Energy Loss (Sn). This kind of process is observed for energies in the energy window below 100 keV.

Both of them independently contribute to the total rate of energy loss. Representing the detector density with ρ (kg/m^3), dE/dx (keV/μm) for the incoming particle energy deposition per unit length, the following equations applies:

$$S_e = \frac{1}{\rho}\left(\frac{d}{dx}E\right)_x \tag{2}$$

$$S_n = \frac{1}{\rho}\left(\frac{d}{dx}E\right)_n$$

A variation of the energy-loss taking place during charged particles absorption exists and follows a curve in which S_e and S_n have a maximum at a given incident energy. These curves can be obtained using values estimated by SRIM-2010 code (Ziegler et al, 1985); for alpha particles absorption in PADC, a typical result is given in Fig. 1,

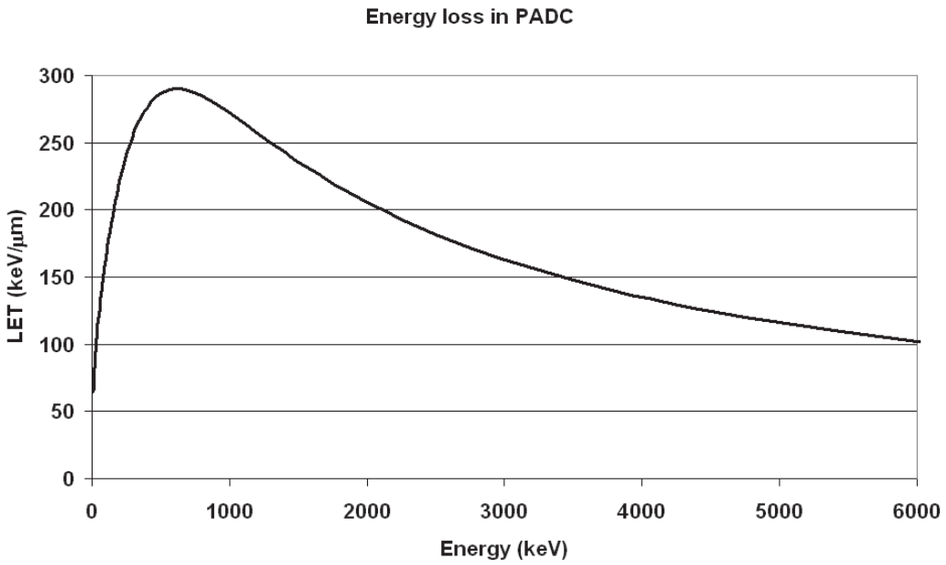

Fig. 1. Specific energy-loss (keV/μm) vs. alpha particle energy taking place during alpha particles absorption. The curve is the sum of S_e and S_n. Similar behaviour for any other absorbing material is expected.

The track etch rate along the particle path shows a similar feature according to the Bragg low as presented in Fig. 2.

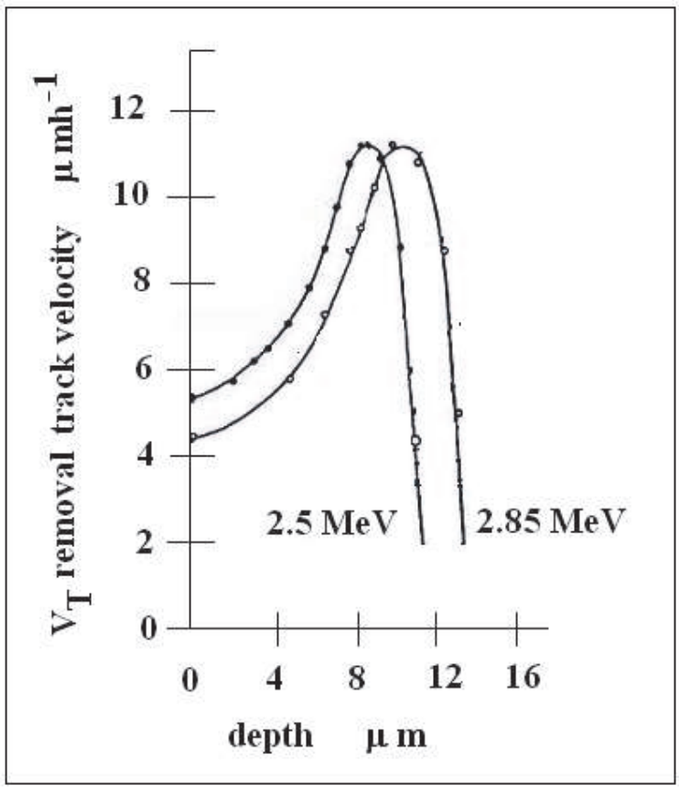

Fig. 2. Bragg ionizing curve for alpha particles of different energies in PADC as observed in the track etch rate, V_T, vs depth in the detector (adapted from Dörschel at al., 2002).

We may observe from Figure 2 that the charged particle entering the detector surface initially transfers energy with a low rate then with an increasing rate, after reaching a maximum value near the end of its path, it drops abruptly to zero. Along the alpha particle path the induced charge density is not uniform due to the Coulomb explosion. This produces a non linear damage in the detector and it has to be taken into account if a precise etching model has to be developed.

4.2 Passive NDT response to charged particle and chemical etching

Due to the dielectric property of PADC detector, molecular polarization and ion diffusion takes place under a high gradient charge concentration. Particles move along an imaginary radius ionizing more molecules and even destroying layers cross-links. As the electrons has a major mobility drift immediately, the heavy positive ions moves at lower velocity and under the action of Coulomb force repulsion intervene and may displace and further ionize atoms favouring interstitial positions. During the short time of the process, also a relaxation effect (ion-hole recombination) takes place. For instance, 6 MeV alpha particle produce 150,000 ion pairs so that the PADC damaged zone that may reach atoms farther that 35 - 40 μm. The ion production is estimated to be around 3–4 ions pairs/nm, that may explain the ionization-density of molecules on its pathway.

The NTD surface absorbs during the process also oxygen from air interfering with relaxation process and therefore has an observable effect on the latent track formation. Several authors suggest that oxygen has an important role. It has already been observed that also the CO_2 gas influences has to be taken into account in making the latent track model. During the energy transfer, temperature gradient (abrupt cooling) increasing the entropy favouring disorder and possibly atomic cluster (amorphous state) formation.
The damage induced on the detector surface can be visualized also by Atomic Force Microscope and the surface opening of the latent track can be measured. (see Figure 3)

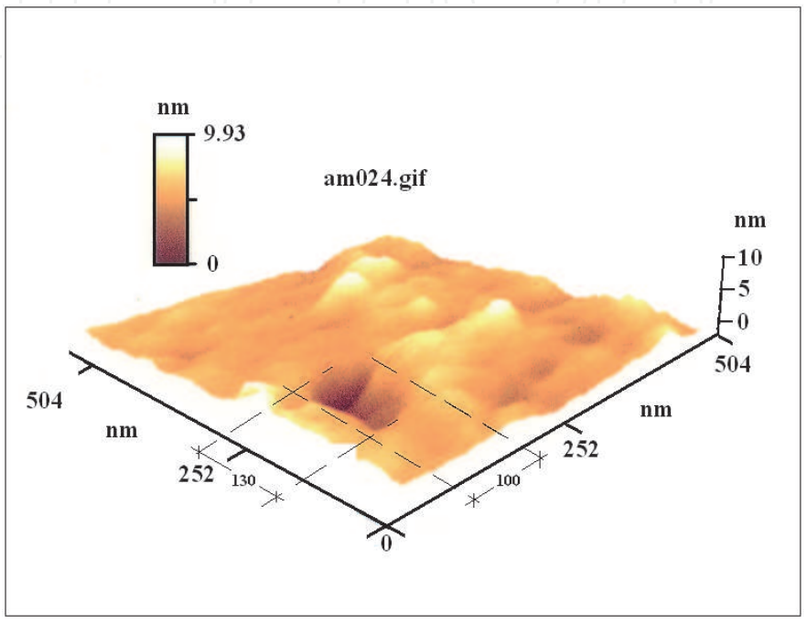

Fig. 3. AFM obtained image of a alpha induced latent track on the detector surface. Dimensions are in nm; alpha source is ^{241}Am, (picture taken by the authors)

Consequently having a proper detector material and analytical equipment with a convenient resolving power (e.g. AFM), the alpha particle fingerprint can be analyzed to obtain physical information. Since this method to analyze the latent track directly is time consuming, consequently unpractical, the latent track opening should be enlarged by chemical process which is the most often employed method.
Among a large group of NTD materials useful to detect charged particles we mention only one of the most sensitive material: called CR-39 ™ discovered by Cartwright et al., (1978), its chemical composition is polyallyl-diglycol-carbonate, PADC. Later, based on this PADC monomer many other products have been developed, more or less with the same properties. NTDs have an important property: that the damaged and the undamaged volume in the detecting materials, under chemical etching behave differently. This is an important property since it provides the possibility to recognize the region where alpha particle impact occurred. To determine the deposited energy it is essential to determine at first the bulk etch rate, V_B. To determine the V_B several experimental techniques have been suggested and a comprehensive report is given by Nickezic et al. (2004). For instance, assuming that the track etch rate is not changing quickly along the path of the perpendicularly incident particle, the following equation for the track diameter, D, is valid (Somogyi, 1973):

$$D = 2h\sqrt{\frac{V-1}{V+1}} \tag{3}$$

In which $V = V_T/V_B$ and h is the thickness of the removed layer during etching. Exposing the detector to very high LET particles as fission fragments we may apply the approximation V >> 1, and then the equation simplifies:

$$D \cong 2h = 2V_B t \tag{4}$$

Here t is the etching time and the V_B parameter can be determined.
Figure 4 shows examples of etched tracks incident on the detector perpendicularly and obliquely and the important, measurable track parameters as: major and minor axes (a, b) and the depth of the peak of the track (L). Also the projected track length is measurable (not marked). They can be used to determine the track etch rate, the incident angle and the real track length. From which, applying appropriate calibration the LET of the incident particle can be deduced (Pálfalvi, 2009).

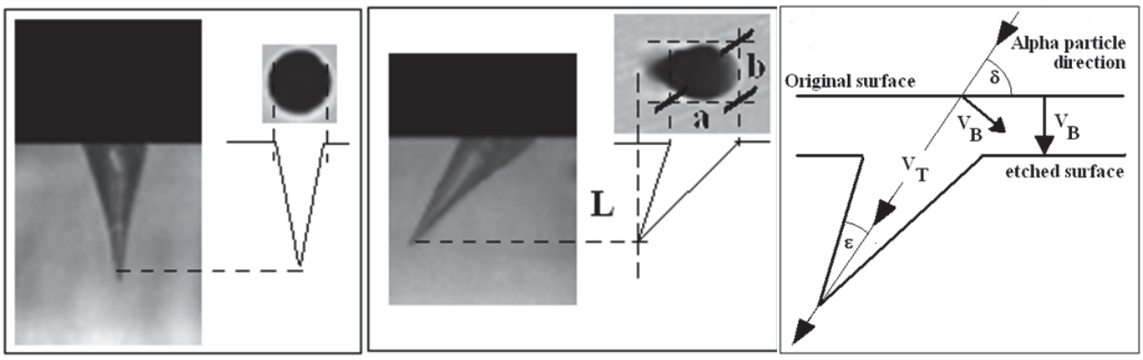

Fig. 4. Side and top views of etched tracks visualized by a light transmission microscope: a and b are the major and minor axes, respectively, L is track depth. V_T and V_B are the track and bulk etch rates, δ and ε are the incident and cone angles.

The size of the track opening (or pit size) depends on the detector material and etching conditions. For a real case when PADC detector (TASTRAK, TASL Co Ltd, Bristol, UK) is used for detecting alpha particles from the ^{10}BNC reaction, usually as control, a standardized, and collimated ^{210}Po alpha source is used, having an energy of 4.6 MeV (Szabó et al, 2002). If the etching is done in 6N NaOH at 70 °C, which results in a bulk etch velocity of V_B =1.34 ± 0.06 μm/h (Hajek et al. 2008), then the track parameters are as summarized in Table 1.

Etching time, h	6
Removed layer, μm	8.0
Track length, μm	18.0
Diameter, μm	10.53
Area, μm^2	87.04
V= (V_T/V_B)	2.55
Range in H_2O, μm	32.2
LET_∞ in H_2O, keV/μm	96.9
Range in PADC, μm	25.8
LET_∞ in PADC, keV/μm	121.5

Table 1. Reference data for control exposures by a standardized ^{210}Po alpha source.

While the averaged track etch rate, V_T, can be determined from Equ (5), for perpendicularly incident particles, when the incident angle, $\Theta = 0°$, in the case of oblique incidence the situation is not so simple. If the incidence angle measured is too high, then the track can be removed during the etching process, therefore, to establish the real number of incident alpha particles the critical detection angle, Θ_c, is introduced which is used then for correction purpose.

According to the "classical method" it is assumed that the V_T is constant along the particle path inside the detector material. If we accept this then the track and bulk etch rate ratio, $V=V_T/V_B$, can be calculated by the following formula (Durrani et al., 1987):

$$V = \frac{\sqrt{\left(1-B^2\right)^2 + 4A^2}}{1-B^2}, \tag{5}$$

where $A = \frac{a}{2h}$ and $B = \frac{b}{2h}$ (a is the measured major-, b is the minor axis, h is the etched off layer thickness, $h=V_B t$, t is the etching time). For the critical angle then the following formula is valid:

$$\cos^2 \Theta_c = \frac{V^2 - 1}{V^2} \tag{6}$$

In the case of isotropic radiation field, the differential alpha particle fluence at a given point x is defined by the next formula :

$$\Phi(\Omega, x) = \frac{d^2 N}{dA d\Omega}, \tag{7}$$

then considering the relation between the critical and the detection angles as shown in Figure 5, the fluence can be deduced (in detail see Benton 2004)

$$\Phi(\Omega, x) = (A 2\pi \cos^2 \Theta_c)^{-1} N, \tag{8}$$

here A is the area of detector where the detected particle number is N.

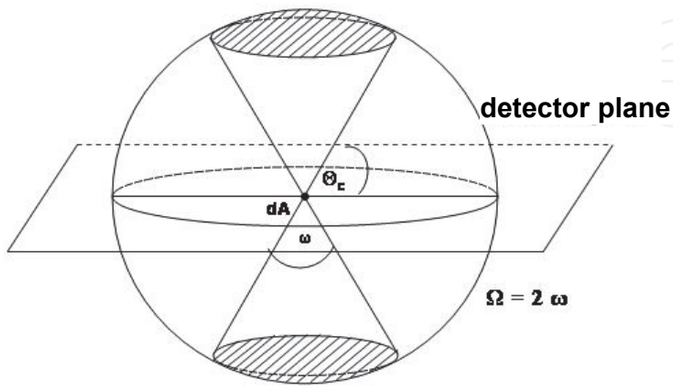

Fig. 5. Assuming isotropic radiation field solid angle (Ω) is determined by the critical angle (Θ_c). Those particles crossing the shaded spherical area and incident on detector area dA will be detected (Palfalvi, 2009).

We draw attention on the fact that PADC detector sensitivity may suffer also from environmental effects. In fact its recording properties change with storage time. It is observed that the registration property is influenced by the presence of oxygen or electron donor gases, even too low or high temperature is influencing it as shown in Figures 6 and 7, where the PADC detectors were exposed to alpha particles. In Figure 6, it is clearly seen from the increasing track area distribution that cooling enhances the registration ability. This is because of the cooling "freezes" the free radicals preventing their recombination. In opposite in Figure 7, the vacuum, the lack of oxygen, decreases the track area, because the oxygen cannot block the recombination of radicals and the damaged zone becomes smaller.

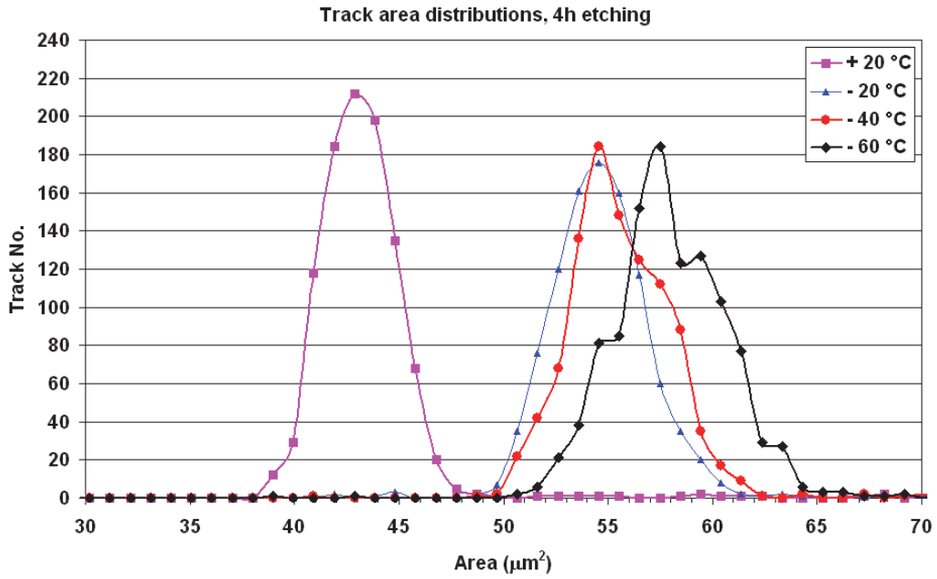

Fig. 6. The effect of the detector cooling on track area distribution (Palfalvi, 2011).

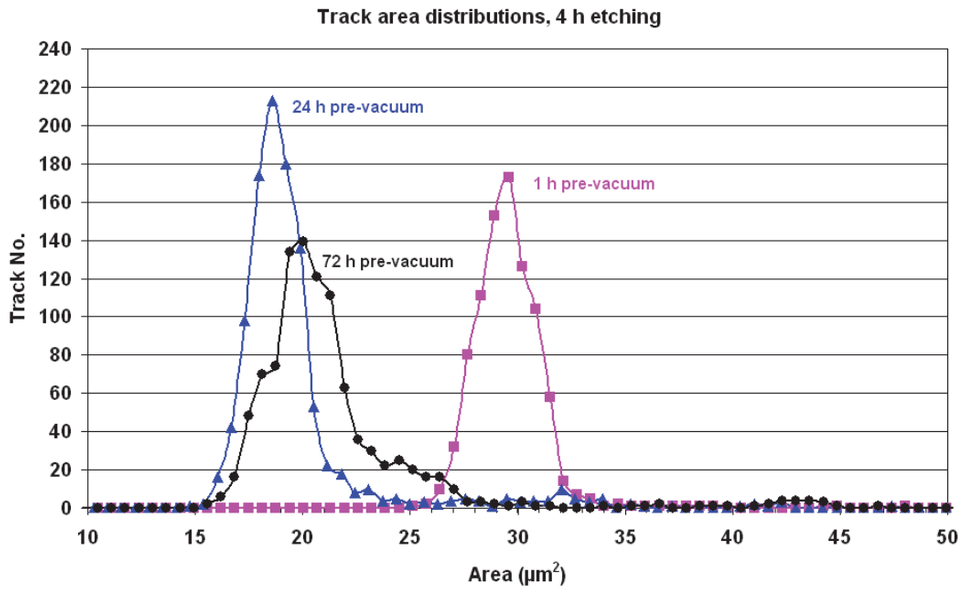

Fig. 7. ^{210}Po alpha track area distributions when vacuum of different durations were applied before exposure (Palfalvi, 2011).

It is important to consider that alpha particles emerge from a thick source with different energies due to self absorption and the track length and diameter depend on it.

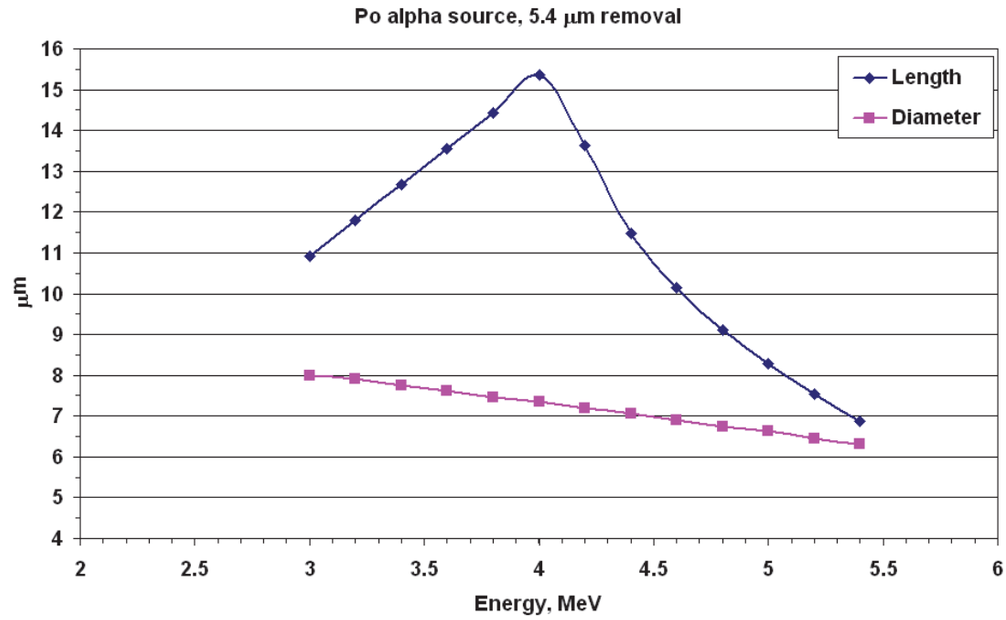

a)

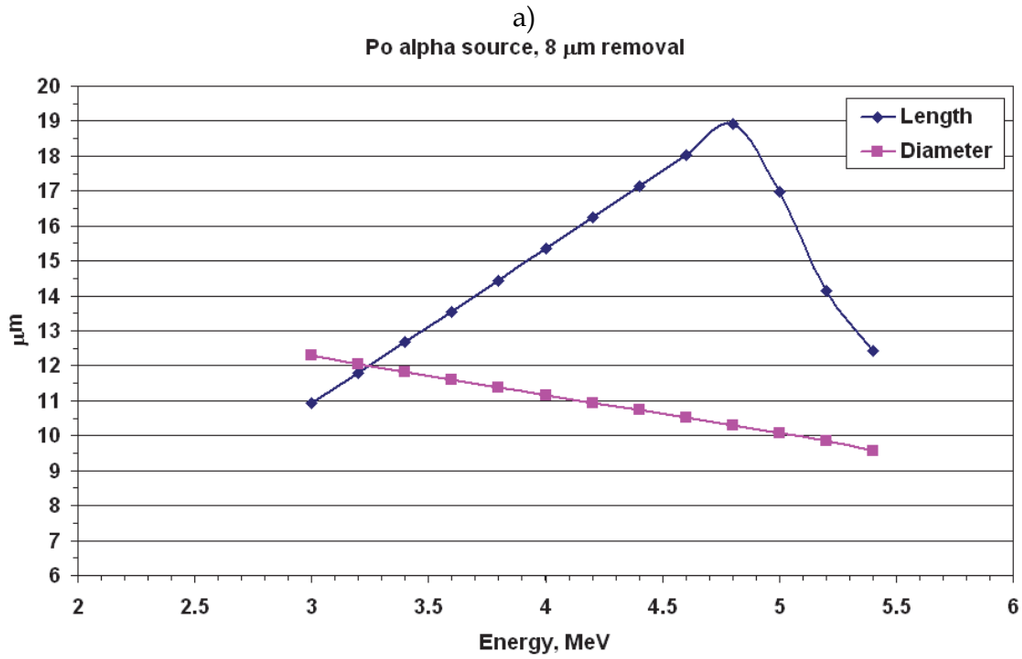

b)

Fig. 8. a and b. PADC response curve to alpha particles with different energies. Curves were obtained after removing by etching 5.4 and 8 mN layers (Palfalvi, 2011).

The data on Figure 8 a and b, have an important role when the source is embedded in a material and the determination of the average depth from where the alpha particle comes is necessary. Sato (2008).

4.3 Automated track counting and software

Commercial and purpose made programs for automated track counting and analysis have been developed and upgraded regularly. A digital image analyser system essentially is a multi component unit, consisting of an optical microscope equipped with a CCD camera, a frame grabber and an analogue-to-digital converter to digitalize the image for further analysis. The microscope stage, the autofocus function and image analyzer are commanded by a purpose made software. Track parameters are obtained from these digital images employing a sequence of functions including mathematical approach for decomposing of multiple overlapping tracks. In most cases the track analysis process is to replace the human eye and its recognition capability, however, operator practice and training is needed even if sophisticated shape recognition method is available. Several custom made automated track counting and related software are reported in the literature, Espinosa et al. (1996), Palfalvi et al. (1997), Patiris et al. (2006), Coppola et al. (2009). A general overview on this subject is given by Hulber (2009).

A typical image of etched tracks obtained by a commercially available system is given in Figure 9. Together with the digitalized image, on the left side of the screen the macro for image analysis is shown. The tracks identification sequence for track parameterization (or macro) was assembled by Gonzalez (2010) employing LabView operating tool.

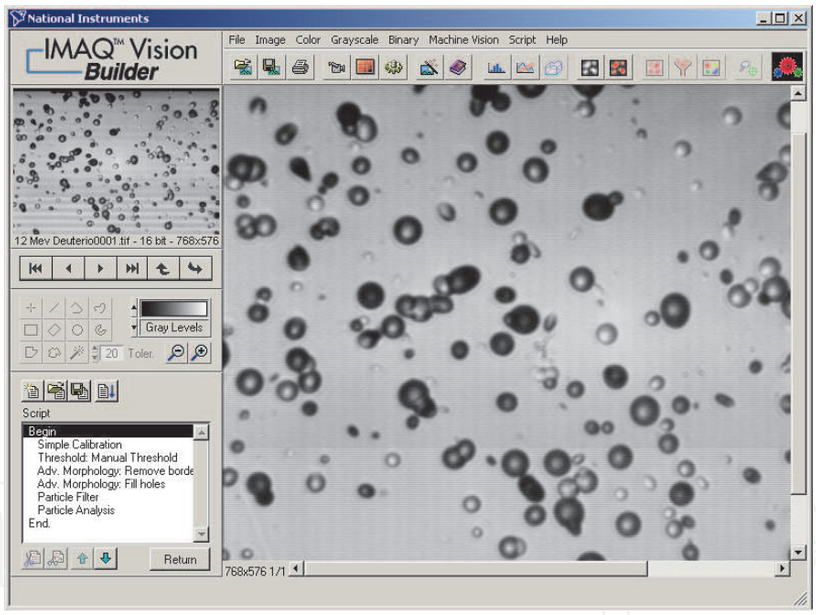

Fig. 9. Digitalized etched tracks as viewed by a commercially available NDT analyzer, Gonzalez (2010).

Once the digitalized image is obtained and unwanted background is eliminated the track perimeter, area, major and minor axes among others quantities are determined. For a given etching time the track position is defined by the (x, y) coordinates (Figure 10.), if etching is continued the same but enlarged track can be located and the new track opening may be observed and the increase of the track length along the third coordinate z can be measured which provides information on the track etch rate. This is relevant when reactions occurs inside the PADC e.g. (n,p) scattering on H atoms or (n,3α) reaction with C nuclei.

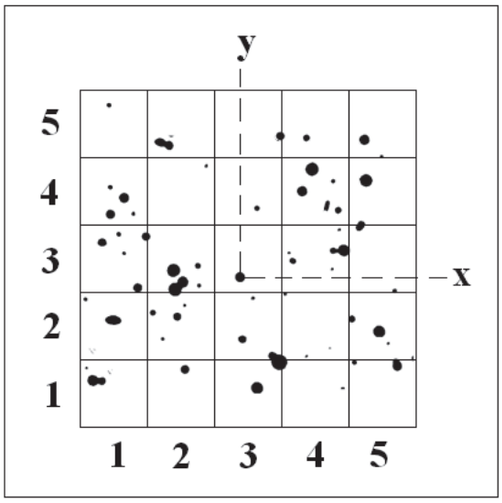

Fig. 10. Typical alpha particle etched tracks in PADC detector. Track diameter is related to the impinging energy, hence the difference in size. Track position is given by (x,y).

The software classifies the tracks on the basis of galleries composed of sample digital images with pre-selected shape and size. In Figure 11 a typical classification of track-openings are shown when the detector was exposed to a plane ^{241}Am alpha source being in a few cm

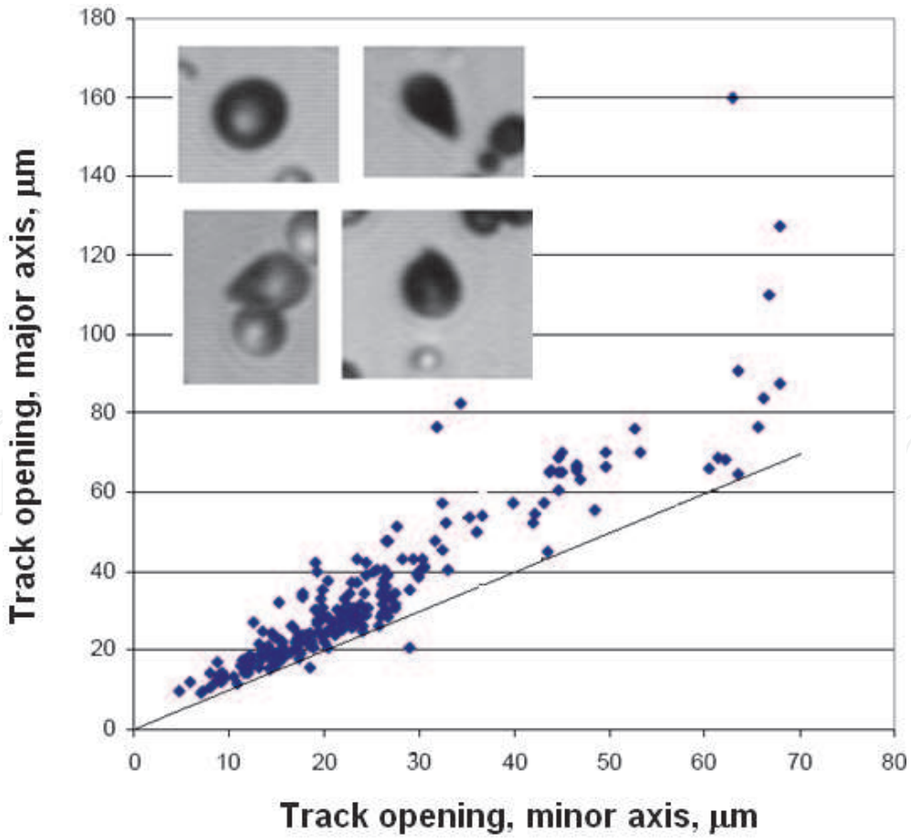

Fig. 11. Elliptical etched tracks distribution with related micrographs.

distance from the detector. The track size covers a large range between 10-70 μm. We may observe also, that a large number of particles have similar energy (15-30 μm) and only few are out of this range with incident angle near the critical one. The continuous line on Figure 14 is drawn to show where the circular tracks would be located. Below the mentioned line we still observe the presence of few tracks (negligible number), however their minor axis seems to be larger than the major axis indicating a false track registration. Similar picture can also be seen when studying alpha emission from a boron loaded sample exposed to neutrons if the ^{10}B bulk density is not uniformly distributed in the volume of the sample, but most atoms can be found in few μm below the surface.

A common feature among software based analyzers exists: all of them contain different solutions to similar problems. These are related to track identification and to pattern characterization including geometric parameters, approximations and software correction. To collect for example tracks into specific groups (discriminated by shape, size, area), chained mathematical and morphologic operations are necessary.

4.4 Control of etching with an alpha irradiation facility

Both the bulk and track etch rate depends on the etching conditions: concentration and temperature. To keep these quantities constant requires special attention, since few tenths of degree change in the temperature can affect the measure of the removed layer, which is responsible for the track etch rate, as seen from the Equ. (5). Usually, the control of the etching procedure is performed by exposing few detectors to alpha particles and measuring the track diameter after the etching. A simple facility can do the exposure with varying alpha energy as shown in Figure 12. The distance between the source and the detector can be adjusted and by this way the alpha energy can be changed. The source here is ^{210}Po, deposited onto a silver plate and placed into a copper holder and covered by a collimator which ensures the perpendicular incidence on the detector (Szabo et al., 2002).

A standard series of track diameters on the dependence of alpha energy and for different etching conditions can be experimentally obtained, which helps to check whether an etching is performed as required or planned.

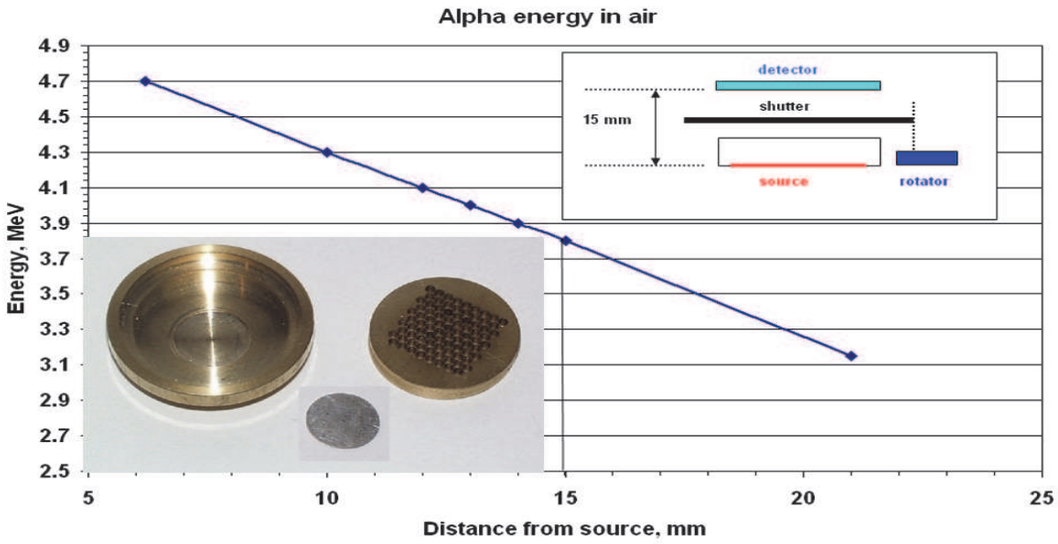

Fig. 12. Alpha exposure facility and the relationship between source-to-detector distance.

For instance, assuming a following relationship between the removed layer, h, and the measured circular track diameter, d, h = c * d, where c is a constant,and applying the data from Table 1, valid for a given detector material and etching, we may obtain for c a value of 0.7567, hence, h = 0.7567*d. So, for a given etching if the h differs from the pre-calculated one, here 8 μm, then the etching was not normal (Palfalvi, 2011).
Several kind of ^{210}Po-based alpha-particle irradiator either for calibration experiments or research have been reported in the literature, Sovland et al., (2000),. Zareena et al., (2008) reported an irradiation procedure and geometry that allows easier dose calculations for blood cells, biological culture or media in a sterile environment. Garty et al., (2005)proposed a novel microbeam facility for biological irradiation studies. Dosimetric characterisation of a simple irradiation device is given by Szabo et al., (2002). A calibration protocol for boron bio-distribution by autoradiography has been developed by Skvarc et al., (2002). Digital images of borated chicken liver and freeze-dried mouse tissue samples were evaluated for boron concentration on the basis of etched track densities in NTD type. Alfassi et al., (1999).

5. Selected examples of ^{10}BNC-reaction applications with PADC

PADC track etch detector (e.g. TASTRAK http://www.tasl.co.uk/tastrak.htm) are frequently applied for alpha particle detection. All the theoretical and experimental investigations resulting from the NDT method, is of great advantage not only in science and technology development but also for industrial application, Pálfalvi et al., (2010). Here we report some examples where the nuclear alpha-radiography by ^{10}BNC-reaction importance is highlighted.

5.1 Neutron field detection, monitoring and dosimetry

Monitoring and detecting of neutron fields, e.g. for nuclear reactor studies, consists of a (n,α) converter material, such as the binary glass metal strip $Fe_{75}B_{25}$, superposed on an alpha particle NTD detector LR 115 film wrapped in cadmium sheets. These NTD-converters are assembled in a stack on acrylic support, Pálfalvi, (1984) Detectors, purchased from DOSIRAD, France (http://dosirad.pagespro-orange.fr/soc_a.htm), consist of an active layer of red cellulose nitrate of 12 μm on a clear polyester base substrate of 100 μm. Although this detector is notcapable of providing information on track parameters mentioned earlier, it can be still useful because only the etched track density determination is needed.
The thermal neutron flux Φnt is determined by the well-known equation:

$$\Phi_{nt} = \frac{W(\rho - \rho_{Cd})}{K\rho_{Fe_{75}B_{25}} N_A f\sigma e^{\sum_x} B t_{irr}} \tag{9}$$

where K is the calibration coefficient, W the atomic weight of boron, ρ and ρ_{Cd} are the track densities without and with cadmium cover, respectively, $\rho_{Fe75B25}$ is the binary glass density, N_A Avogadro's number, f the ^{10}B isotopic abundance in the $Fe_{75}B_{25}$, σ the cross section of the ^{10}B(n,α)^{7}Li reaction, $e^{-\Sigma x}$ the neutron average attenuation in the $Fe_{75}B_{25}$, B the yield quotient of the reaction and t_{irr} the irradiation time. The track density is obtained by etched track analysis Pálfalvi, (1982); it therefore provides the neutron field intensity near the energy region of thermal or cold neutrons Pálfalvi, et ali., (2001). The method is particularly useful to determine anisotropy of thermal neutron flux of graphite, heavy water or polyethylene moderated RINS such ^{252}Cf, ^{241}Am-Be or others (Alvarado et al., 2010).

The dose due to presence of high energy neutrons can be determined by PADC detectors Sainz et al., (2004), Santa Cruz et al., (2004). The technique requires several etching steps and individual track evaluation. In this case an automated analyser system is required. The technique provides neutron ambient dose equivalent (H*) between 200 keV and 20 MeV. It was applied with success at the International Space Station where values were reported in the range of 39 to 73 μSv/d, with an uncertainty estimated to be around ± 30 %, Pálfalvi (2004). PADC- CR39 coupled with a boron converter is employed currently as passive neutron "rem counter" as reported by Agosteo et al., (2010); essentially the device is a polythene designed to determine ambient dose equivalent conversion coefficients, H*(10)/F, for a broad energy window 0.025 eV - 1 GeV. Dose related study and its importance is given by Stap (2008).

5.2 Isotopic ^{10}B density determination

For low particle fluencies that induce well defined circular etched track without overlapping, a strong linear correlation exists between track density and particle yield. As the track density increases overlap cannot be avoided and density determination is less precise. However assuming an intermediate interval where track density and the overlapping frequency optimize, the etched track method demonstrated to be reliable and a non destructive procedure e.g. for:

i. Determination of the boron either surface or bulk concentration in any given sample.
   - ^{10}BNC-therapy. In this case, ^{10}BNC-reaction to be an effective technique in cancer treatment ^{10}B –bio distributions has to be known. The method of alpha-radiography is applied e.g. in sliced whole-body of tumour analysis as well as in cancerous cells in rat's brain, kidneys and liver. Occasionally a mixture of boric acid and borax compound medium is employed as carriers and ^{10}B is determined in microtome samples positioned between two pieces of NTD (Wittig et al., 2008).
     Etched track provides a remarkably good image of the boron density in tissue; see Figure 13 and17.

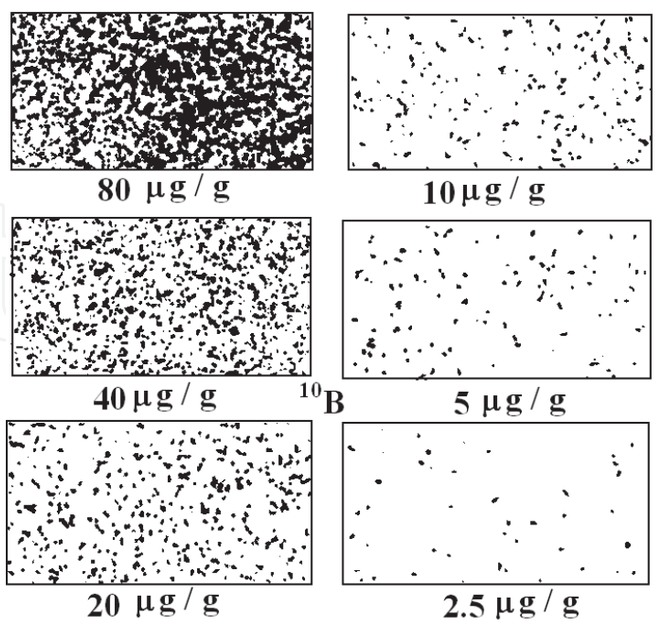

Fig. 13. Alpha radiography of boron in malignant melanoma by NTD. (adapted from Takagaki et al. 1990)

- In vitro study of radiobiological samples under low fluencies of alpha particles. Precise localization of each particle track in a monolayer cell is provided by alpha radiography, as demonstrated by Gaillard et al., (2005). Results evidence that living cell cultures exposed to alpha-radiation (dose rate 2-3 particle/cell/hour) suffer morphological changes Selmeczi et al., (2001). It has been demonstrated also that tracks give important information on the cell migration dynamics.

ii. Study of boron spatial distribution.

Material science studies specifically binary glass metal ($Fe_{75}B_{25}$) have benefited from detailed knowledge of boron distribution. In Figure 14 etched tracks in LR-115 show the non uniform boron distribution where dislocations and its sparse agglomerations can be observed.

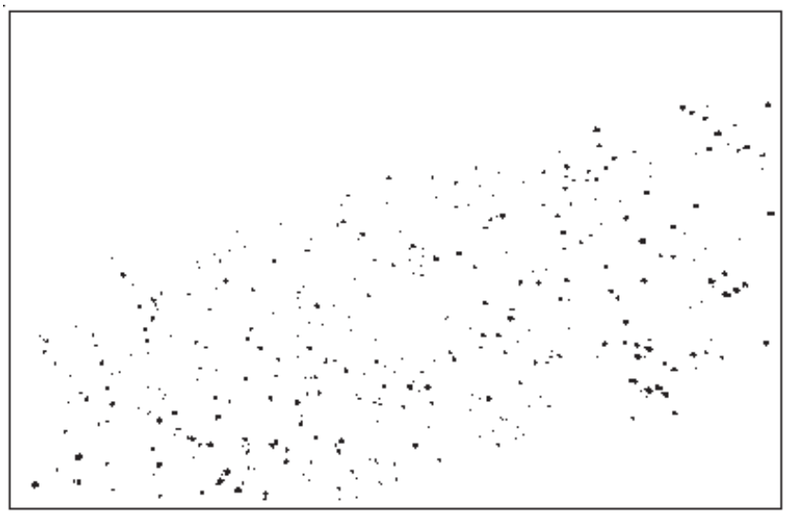

Fig. 14. Glass metal $Fe_{75}B_{25}$, irradiated with neutrons from ^{252}Cf. Spots are the etched alpha tracks (NTD-LR-115) and the metal edges are well recognized.

iii. Lithium-Helium doping of a given Boron-structured material.

Megusar (1983), studied lithium and boron doping techniques to produce displacement or damage in bulk specimens of non-nickel bearing materials employed in fast fission reactors. It was demonstrated that lithium doping has an advantage over boron. Alloys with a stable boron compound uniformly distributed have been already developed and the (n,α) reaction could be a new technique to convert boron to lithium applying the reaction detailed in Equ. 1.

5.3 Gradient of boron concentration in thin film deposition

Local boron concentration and its micro distribution on materials such as polycrystalline beta-silicon carbide, laser ablated B_4C thin films or Mo-Si-B alloys among others have been studied or they will be scrutinized in the future using the (n,α) reaction and employing the NTD PADC, LR-115 or similar passive detectors. Its importance is related to the boron deposition technique and useful information can be derived by alpha auto radiography which may exhibit a large gradient of boron density. The area distribution of alpha tracks (Table 2) can be visualized in 3D as shown on Figure 15. To avoid high density overlapped tracks, it is convenient to calculate the irradiation time (t_{irr}) to obtain around $\rho=10^4$ tracks/cm^2. This can be estimated by the following equation:

$$t_{irr} = \rho(g\sigma_a \Phi N C_B R)^{-1} \quad (10)$$

Where: g is a geometrical factor, with an empirical value of 0.25; σ_a thermal neutron capture cross section for ^{10}B ($7.6x10^{22}$ cm^2); Φ neutron flux ($1.67x10^8$ n/cm^2 s); N atom density of the sample, for boron steel ($8.5x10^{22}$ cm^3); C_B fraction of boron atoms ($1.7x10^4$ for boron standard); $R = R_\alpha\tau_\alpha + R_{Li}\tau_{Li}$ in that R_α, R_{Li} are the ranges of alpha particles and lithium ions respectively; τ_α, τ_{Li} track registration efficiencies for alpha and lithium ions (assumed to be unity).

y / x	1	2	3	4	5	6	7	8	9	10	11	12	13	14
1	3	4	7	6	**15**	6	3	1	2	2	0	0	3	5
2	0	4	1	3	**14**	5	4	**8**	3	3	5	1	0	1
3	4	1	1	1	**10**	6	4	**24**	**10**	**9**	4	5	5	3
4	3	1	0	0	**13**	4	1	**39**	4	5	5	9	3	0
5	6	0	1	0	**14**	5	8	**21**	**9**	3	7	1	5	1
6	1	4	0	0	**17**	**8**	6	**38**	2	4	3	3	3	1
7	5	3	2	0	**21**	**28**	**13**	**30**	5	6	5	4	0	2
8	6	3	0	1	**31**	**20**	**17**	**39**	4	2	5	3	5	2
9	5	1	0	1	**21**	**6**	**41**	**44**	6	0	2	2	2	0
10	5	2	1	0	**20**	**11**	**29**	**40**	3	2	5	3	4	1
11	1	2	0	0	**35**	6	1	**31**	6	5	2	1	3	11
12	1	1	0	0	**23**	3	9	**10**	**28**	4	1	3	4	6
13	1	1	0	1	**14**	12	4	7	**46**	**22**	4	2	7	3
14	1	4	0	0	**46**	4	4	**22**	**44**	3	2	4	1	2
15	1	1	0	0	**46**	3	**18**	**29**	6	4	4	2	0	0
16	1	0	0	0	6	9	2	3	**31**	**39**	4	3	3	4
17	4	2	1	0	0	4	2	4	**18**	**26**	2	1	1	2
18	4	0	0	0	0	3	5	7	**39**	**12**	**11**	3	2	2
19	1	0	2	1	2	0	3	4	**9**	**26**	3	3	2	3
20	2	2	1	0	0	4	4	3	2	5	5	5	2	1
21	3	0	0	0	1	3	5	3	6	3	5	3	2	1
22	2	3	0	0	3	1	2	0	4	5	2	2	1	1
23	0	2	0	0	2	1	6	0	1	4	2	2	1	1

Table 2. Measured track density (given by bolded numbers) localized by numerical coordinates (x,y)

The coordinate number refers to a microscope field view of 100μm x 150 μm area positioned on a plastic detector of the size of 10 mm x 21 mm area. These data are plotted as 3D map by a software program. The resulting hill like map is shown on Figure 15.

In Figure 15 etched track spatial distribution of track density, ρ(x,y) and its gradient is given. 3D map was rendered by Surfer ™. On the left, disposition of glass metal strip as positioned on the NTD is shown. The other information, discerned from the picture or map on the right side, is that the sample edges are sharp and where two samples superimpose the track density does not show an abrupt increase as it would be expected. The main reason is because the alpha particle range is comparable to the sample thickness and self absorption effect reduces sharply track recording.

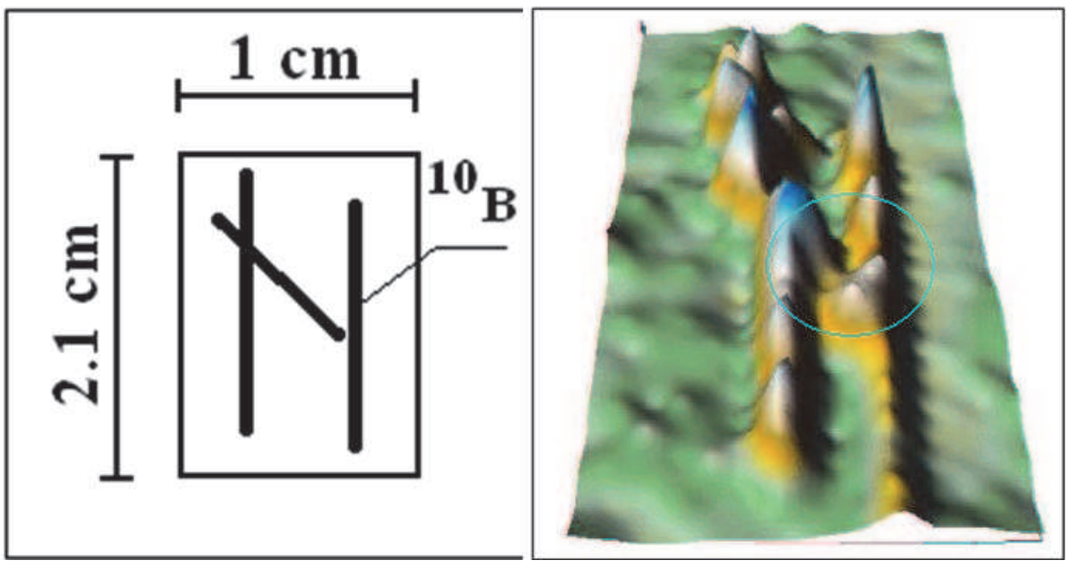

Fig. 15. Overall view of alpha tracks spatial distribution resulting from glass-metal strips ($Fe_{75}B_{25}$) shown as heavier black lines on the left side, detector dimensions are in cm. Circle indicate the place where auto absorption effect is dominant.

It would be interesting to apply the autoradiography methodology to study e.g. micro cracks or fissures due to material fatigue, manufacturing imperfections including micro structural temporal evolution. Where these structural in-homogeneities occur, we would observe track density variation of the type shown in the encircled region of Figure 15.
Important results were obtained studying toughness and ductility in the high-temperature intermetallic compound by etched track mapping of the location of the boron. Results (see Figure 16) supports that it is distributed randomly in (Al–Ru–B) alloys, (Middlemas et al., 2010). Fleisher (2005) observed from alpha radiography on PADC that it is concentrated at grain boundaries, effect that lowers the alloy's shear modulus (see Figure 16)

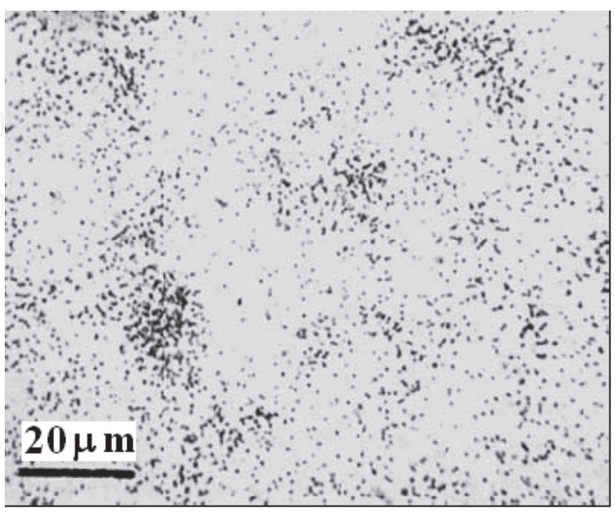

Fig. 16. The etched detectors viewed in a Leitz Ortholux microscope for track distributions at magnifications of 100x (adapted from Fleisher, 2005)

5.4 ^{10}B-Carrier deposition effectiveness in biomedical sample

^{10}B isotope finds application in nuclear medicine and generally in the biophysical field. It has been demonstrated to be an ideal isotope for cancer therapy. The cancerous cells absorb more boron compound than normal cells. Thus applying the ^{10}BNC-reaction the alpha products have the possibility to destroy the tumour without or with low damage to normal tissues. The therapy taking advantage of the method is briefly referred as ^{10}BNC-therapy or simply BNCT. In the literature often it is also referred to as a binary radiation therapy modality. This technique is based on carrier-modality that requires a molecule rich in boron content, having a capability to enter selectively targeted cells. For instance carboranyl groups, called *carrier,* have attached boron atoms e.g. $B_{10}H_{10}$ and $B_{12}H_{12}$ and these compounds can be synthesized to contain only the requested ^{10}B isotope. Other appropriate chemical compounds tagged with ^{10}B (e.g. BPA (boron-phenylalanine) BSH (sulphydril-borane); BOPP (protoporfirina boronated) are currently employed. To take advantage of the disruptive power of the ^{10}BNC-reaction product appropriate neutron irradiations is required. A relatively low dose of thermal neutrons is applied inducing energetic alpha particles and therefore a high density atomic ionization (LET). During the atomic and molecular recombination, chemical structure is modified which in turn, inhibits or disrupts the cell activity. Further advantage is the boron element low toxicity (300 μg/g) and the fact that in bacteria the concentration may already be around 150 (μg/g) B_{nat} suggesting the applicability of ^{10}BNC-reaction as a new analytical technique in oncology. We give some results of the mentioned carrier-modality in biomedical field and later we refer to another method called internal boron-modality. Well understood chemistry of boron allows synthesizing borated drugs or purpose made molecules to provide incorporation techniques into e.g. high-grade gliomas and generally any tumour, (Altieri et al., 2008). In order to establish the effectiveness of these boron carriers it is necessary to determine their distribution e.g. in GS-9L gliosarcoma cells. Several studies point that carrier agents, like p-boronophenylalanine (BPA) distributes relatively homogeneously (Bennett et al., 1994). Recently an important study was completed with ^{10}BNC-therapy at RA-3 reactor facility by Portu et al. (2011), in which histological features have been accurately visualized by alpha etched track density in NTD-Lexan, see Figure 17.

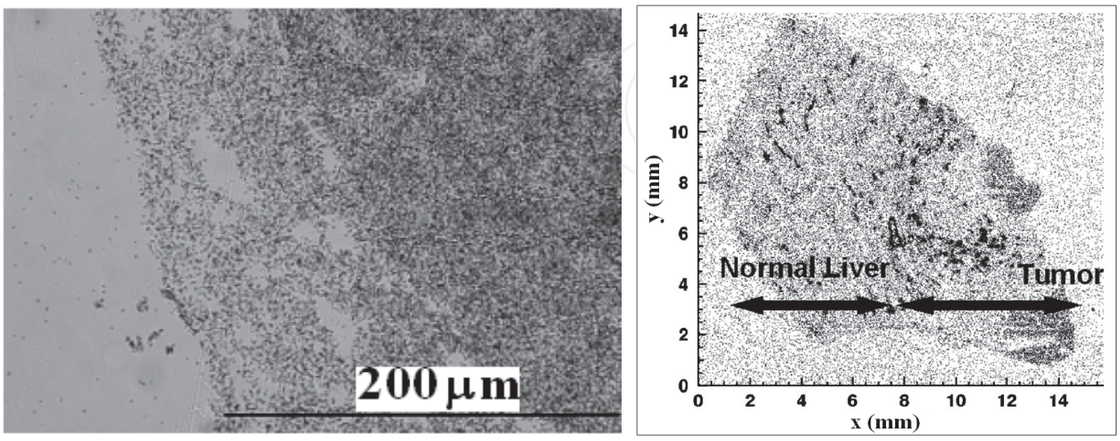

Fig. 17. Alpha autoradiography image of a tumour section (left) adapted from Portu et al. (2011) and on the right ^{10}B distributions in VX-2 tumour that shows selective uptake by intra-arterial injection, (adapted from Mikado (2009)

The other so called internal boron-modality is related to boron content in many naturally occurring bio-samples. Just to mention one, the natural antibiotic such as boromycin, contains elemental boron. The ^{10}BNC-reaction technique could be employed to determine the concentration and its bio-efficiency. As mentioned at the beginning several other substances occur in our environment and the given NTD methodology could be applied in revealing the boron content in many environmental samples.

5.5 Boron mapping in plant physiology

An interesting application for ^{10}BNC-reaction method is related to plant nutrients. It has been recognized that boron is essential for growth performance; in fact then concentration should be in the range of 0.8 - 1.8 ppm. Otherwise poor plant grows or boro soil boron toxicity shows up. Therefore it would be convenient to employ the alpha radiography technique for plant physiology studies; alpha track mapping could detect boron concentrations with values lower than few ng/g. It could be also employed for uptake determination in different parts of the plant. A few studies have already been reported and it can still be considered, from the NDT point of view, as a little explored field.

It seems that the isotopic ratio ^{11}B/^{10}B in this study field, departs from the naturally occurring value. It has been observed that ratio values may change significantly from the expected value of ^{11}B/$'^{10}$B =4.1 depending on the sample taken from different parts of the plants. This kind of isotopic effect related to boron biochemistry foliar processes, indicates that the boron uptake should be studied further (Vanderpool et al., 1992).

5.6 Topics for further application of ^{10}BNC-reaction relevant for environmental monitoring, industry and commercial certifications

Boron is dissolved in surface and underground water other than the sea as a chemical compound e.g. $B(OH)_3$ (aq) or $B(OH)_4^-$ (aq); its concentration is in the range of 4-15 ppm (dry mass) (Water, 2011).

Boron concentration in surface waters comes from minerals with boron concentrations between 5 and 80 ppm; such as kernite, borax, ulexite, colemanite among others. It can be measured even in households as sodium perborate in detergents, eventually damaging the environment. However the boron has an important role in environmental studies; it is an indicator to detect the presence of other hazardous substances. For example, the boron-trifluoride-ethyl-ether complex reacts with water, forming diethyl ether BF_3, and releasing some highly flammable gases. A number of boron compounds, such as boron tri iodide, are hydrolysed in water. Therefore detecting boron by ^{10}BNC-reaction and PADC technique could be important for environmental monitoring.

On the other hand industrial plants with significant B-concentration such as that found in fumaroles pollute the environment with compounds such as boric acid, borates and boron minerals, (Environment, 1998). Often boron compounds are also found in food; for concentration measurement the colorimetric curcumin method is used. That could be replaced by the ^{10}BNC-reaction or autoradiography being simpler and a direct method. It could be applied also in the field of molecular synthesis, (Solozhenko et al., 2009) where this technique could be of advantage including far apart fields such as nano-tube manufacturing (Yu et al., 2006) and human genetics (Vithana et al., 2006).

6. Conclusions

Distribution of ^{10}B in samples raging from medicine to industry from environment to food certification are determined using passive nuclear track detectors and a neutron beam for irradiation. This technique will spread among a larger community as the demand for boron determination increases. For the near future the most important field of application will be environmental monitoring and cancer therapy. Tumour tissue destruction is a health priority and studies will be further extended to improve ^{10}B carriers and boron imaging to visualize microscopic uptake and its distribution in cell or any other material.

7. Acknowledgements

The support received from the INFN (Sezione di Padova) and the University of Studies of Padova is acknowledged. This work was also partly supported by the European Commission in the frame of the FP7 HAMLET project (Project # 218817).

8. References

Agosteo S., Caresana M., Ferrarini M., Silari M.,(2010). A passive rem counter based on CR39 SSNTD coupled with a boron converter. Rad. Meas., 44, 985–987.

Alfassi Z. B., Probst T. U., (1999). On the calibration curve for determination of boron in tissue by quantitative neutron capture radiography. Nucl. Instr. Meth. A 428, 502-507.

Alvarado R., Palacios D., Sajo-Bohus L., Greaves E.D., Barros H., Nemeth P. Goncalves I.F. (2010). Neutron flux characterization using LR-115 NTD and binary glass metal as converter. Rev. Mexicana de Fisica S 56, 5–8.

Altieri, S., Braghieri, A., Bortolussi, S., Bruschi, P., Fossati, F., Pedroni, P., Pinelli, T., Zonta, A., Ferrari, C., Prati, U., Roveda, L., Barni, S., Chiari, P., Nano, R., (2008). Neutron autoradiography imaging of selective boron uptake in human meta- static tumours. Appl. Rad. Isot. 66, 1850–1855.

Bennett B. D., Mumford-Zisk J., Coderre J. A. and Morrison G. H. (1994). Subcellular Localization of p-Boronophenylalanine-Delivered Boron-10 in the Rat 9L Gliosarcoma: Cryogenic Preparation In Vitro. Rad. Res. 140, 72-78.

Benton, E. R. (2004). Radiation Dosimetry at Aviation Altitudes and in Low-Earth Orbit, Ph.D. Thesis, University College, Dublin, Ireland.

Cartwright, B. G., Shirk E. K. and Price, P. B., (1978). A nuclear-track-recording polymer of unique sensitivity and resolution. Nucl. Instr. Meth. 153, 457–460.

Coppola F., Durante M., Gialanella G., Grossi G., Manti L., Pugliese M. and Scampoli P., (2009). Development of an automated scanning system for the analysis of heavy ions' fragmentation reaction by nuclear track detectors. Rad. Meas., 44, 802-805.

Dörschel B., Hermsdorf D. and Kadner K., (2002). Studies of experimentally determined etch-rate ratios in CR-39 for ions of different kinds and energies. Rad. Meas. 35, 183-187.

Durrani, S.A., Bull, R.K., (1987). Solid State Nuclear Track Detection: Principles, Methods and Applications. Pergamon Press, Oxford. p. 284.

Environmental Health Criteria 204: Boron the IPCS. (1998). http://www.inchem.org/documents/ehc/ehc/ehc204.htm.

Espinosa G., Gammage R.B., Meyer K.E. and Dudney C.S., (1996). Nuclear Track Analysis by Digital Imaging. Rad. Prot. Dos., 66, 363-366.

Fleischer R.L., (2005). The distribution of boron in AlRu: Effect on ductility and toughness. Acta Materialia 53, 2623–2627.

Gaillard S., Armbruster V., Hill M.A., Gharbi T., Fromm M., (2005). Production and validation of CR-39-based dishes for alpha-particle radiobiological experiments. Rad. Res. 163, 343-350.

Garty G., Rossi G. J., Bigelowa A., Randers-Pehrson G., Brenner D. J. (2005). A microbeam irradiator without an accelerator. Nucl. Instr. Meth. B, 231, 392-396.

Gonzalez (2010), Private Communication.

Hajek, M., Berger, T., Vana, N., Fugger, M., Pálfalvi, J.K., Szabó, J., Eördögh, I., Akatov, Y. A., Arkhangelsky, V. V. And Shurshakov, V. A., (2008). Convolution of TLD and SSNTD measurements during the BRADOS-1 experiments onboard ISS (2001). Rad. Meas. 43, 1231-1236.

Hulber E. (2009), Overview of PADC nuclear track readers. Recent trends and solutions Rad. Meas., 44, 821-825.

Leung, K. (2002) U.S. Patent #6,907,097.

Lounis Z., Djeffal S., Morsli K. and Alla M. (2001). Track etch parameters in CR-39 detectors for proton and alpha particles of different energies. Nucl. Instr. Meth. B: 17, 543-550.

Megusar J., Harling O.K. and Grant N.J. (1983). Lithium doping of candidate fusion reactor alloys to simulate simultaneous helium and damage production. J. Nucl. Mat., 115, 192-196

Middlemas M.R. (2010), http://www.lbl.gov/ritchie/Programs/Moly/Moly.html.

Mikado S., Yanagie H., Yasuda N., Higashi S., Ikushima I, Mizumachi R., Murata Y., Morishita Y., Nishimura R., Shinohara A., Ogura K, Sugiyama H., Iikura H., Ando H., Ishimoto M., Takamoto S., Eriguchi M, Takahashi H., Kimura M., (2009). Application of neutron capture autoradiography to Boron Delivery seeking techniques for selective accumulation of boron compounds to tumor with intra-arterial administration of boron entrapped water-in-oil-in-water emulsion. Nucl. Instr. Meth. A 605, 171–174.

Naranjo B., Gimzewski J.K. and Putterman S., (2005). Observation of nuclear fusion driven by a pyroelectric crystal. *Nature* 434, 1115-1117.

Nikezic D. and Yu K.N., (2003). Calculations of track parameters and plots of track openings and wall profiles in CR-39 detector. Rad. Meas. 37, 595-601.

Nikezic D. Yu K.N., (2004). Formation and growth of tracks in nuclear track materials Mat. Sci. and Eng. R 46 51–123.

Pálfalvi, J. K., (1982). Neutron Sensitivity of LR-115 SSNTD Using Different (n,alpha) Radiators, Nucl. Instr. Meth., 203, 451-457.

Pálfalvi, J. K. (1984), Neutron Sensitivity Measurements of LR-115 Tracks Detector with Some (n,alpha) Converters, Nuclear Tracks, 9, 47-57.

Pálfalvi J. K., Eordog, I., Szabo,J. and Sajo-Bohus L., (1997). A new generation image analyser for evaluating ssntds. Rad. Meas. 28, 849-852.

Pálfalvi J. K., Sajó-Bohus L., M. Balaskó and I. Balásházy (2001). Neutron field mapping and dosimetry by CR-39 for radiography and other applications. Rad. Meas. 34, 471-475.

Pálfalvi, J. K., Akatov, Y. A., Szabó, J., Sajó-Bohus, L. and Eördögh, I., (2004). Evaluation of SSNTD Stacks Exposed on the ISS. Rad. Prot. Dos. 110, 393-397.

Pálfalvi J. K., (2009). Fluence and dose of mixed radiation by SSNTDs: achievements and constrains. Rad. Meas. 44, 724-728.

Pálfalvi J. K., Szabó J. and Eördögh I., (2010). Detection of high energy neutrons, protons and He particles by solid state nuclear track detectors. Rad. Meas., 45, 1568-1573.

Pálfalvi J. K., (2011). Unublished, private communication.

Patiris D.L., Blekas K., Ioannides K.G., (2006). TRIAC: A code for track measurements using image analysis tools. Nucl. Instr. Meth. 153, B 244, 392–396.

Persaud A., I. Allen, M. R. Dickinson, T. Schenkel, R. Kapadia, K. Takei and A.Javey, (2011). Development of a compact neutron source based on field ionization processes. American Vacuum Society. DOI: 10.1116/1.3531929.

Portu A., Carpano M., Dagrosa A., Nievas S., Pozzi E., Thorp S., Cabrini R., Liberman S., SaintMartin, G., (2011). Reference systems for the determination of ^{10}B through autoradiography images: Application to a melanoma experimental model. Appl. Radiat.Isotopes, DOI:10.1016/j.apradiso.2011.02.049.

Sainz C., Soto, J., Casado, J., Bueren, J., (2004). Effects on CD34+ haematopoietic stem cells induced by low doses of alpha irradiation. Int'l J. Low Radiation 2, 208 – 215.

Santa Cruz GA, Zamenhof L., (2004). The microdosimetry of the ^{10}B reaction in boron neutron capture therapy: a new generalized theory. Rad. Res. 162, 702-10.

Sato F., Kuchimaru T., Kato Y. and Iida T., (2008). Digital Image Analysis of Etch Pit Formation in CR-39 Track Detector. Jpn. J. Appl. Phys. 47 269-272.

Selmeczi D., Szabo B., Sajo-Bohus L., Rozlosnik N., (2001). Morphological changes in living cell cultures following α-particle irradiation studied by optical and atomic force microscopy. Rad. Meas., 34, 549-553.

Skvarc, J., Giacomelli, M., Yanagie, H., Kuehne, G., (2002). Selective radiography of 10B distribution in organs using cold and thermal neutron beams. Cell Mol Biol Lett.,7, 162-4.

Solozhenko, V.L., Kurakevych, O.O., Le Godec, Y., Andrault D., Mezouar, M., (2009). "Ultimate Metastable Solubility of Boron in Diamond: Synthesis of Superhard Diamondlike BC5". Phys. Rev. Lett. 102: 015506.

Somogyi G. and Szalay, S.A., (1973). Track-diameter kinetics in dielectric track detectors. Nucl. Inst. Meth. 109, 211-232.

Søyland C, Hassfjell S. (2000). A novel ^{210}Po-based alpha-particle irradiator for radiobiological experiments with retrospective alpha-particle hit per cell determination. Rad. Environ. Biophys. 39, 125-30.

Stap J., Krawczyk P., Van Oven C, Barendsen G, Essers J, Kanaar R, Aten J.,.(2008).Induction of linear tracks of DNA double-strand breaks by alpha-particle irradiation of cells. Nat. Meth.. 5, 261-266.

Stevanato L., Caldogno M., Dima R., Fabris D., Hao X., Lunardon M., Moretto S., G. Nebbia G., Pesente S., Sajo-Bohus L., and Viesti G., (2010). A new facility for Non-Destructive Assay with a time-tagged ^{252}Cf source. AIP Conf. Proc., 4, 1265, 431-434.

Szabo J., Feher I., Pálfalvi J., Balashazy I., Dam A.M., Polonyi I., Bogdandi E.N., (2002). In vitro cell irradiation systems based on 210Po alpha source: construction and characterisation. Rad. Meas., 35, 575-8.

Takagaki M. and Mishima Y., (1990). Boron-10 quantitative analysis of neutron capture therapy on malignant melanoma by spaectrophotometric alpha-track reading. Nucl. Tracks Rad. Meas. 17, 531-535.

Vanderpool R.A., Johnson P.E. (1992). Boron isotope ratios in commercial produce and boron-forliar and hydroponic enriched plants. J. Agric. Food Chem. 40 (3), pp 462-466

Vithana E., Morgan P., Sundaresan P., Ebenezer N., Tan D., Mohamed M., Anand S., Khine K., Venkataraman D., Yong V., Salto-Tellez M., Venkatraman A., Guo K., Hemadevi B., Srinivasan M., Prajna V., Khine M., Casey J., Inglehearn C., Aung T. (2006). "Mutations in sodium-borate cotransporter SLC4A11 cause recessive congenital hereditary endothelial dystrophy. Nat. Genet. 38, 755 – 757.

Water (2011), http://www.lenntech.com/periodic/water/boron/boron-and-water.htm#ixzz1LDAyFUVO and references therein.

Wikipedia (2011), http://en.wikipedia.org/wiki/Boron, and refrences therein.

Wittig A., Michel J., Moss R.L., Stecher-Rasmussen F., Arlinghaus H.F., Bendel P., Mauri P.L., Altieri S., Hilger R., Salvadori P.A., Menichetti L., Zamenhof R., Sauerwein W.A., (2008). Boron analysis and boron imaging in biological materials for boron neutron capture therapy (BNCT). Crit. Rev. Oncol. Hematol. 68, 66–90.

Yu J., Ying C., Elliman R. G., Petravic M., (2006). Isotopically enriched ^{10}B nanotubes. Adv. Mat., 18, 2157-2160.

Zareena Hamza, V., Vivek Kumar P. R., Jeevanram R. K., Santanam R., Danalaksmi B. and Mohankumar M. N., (2008), A simple method to irradiate blood cells in vitro with radon gas, Rad. Prot. Dos. 1–8.

Ziegler James F., Ziegler M.D., and Biersack J.P., (2010). SRIM - the stopping and range of ions in matter. Nucl. Instr. Meth. B 268, 1818–1823.

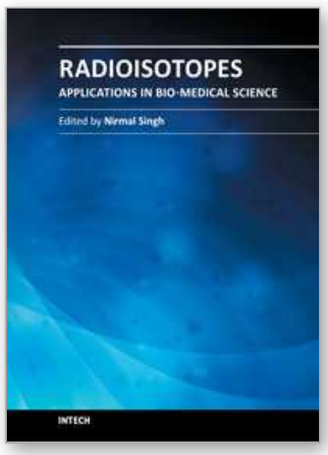

Radioisotopes - Applications in Bio-Medical Science
Edited by Prof. Nirmal Singh

ISBN 978-953-307-748-2
Hard cover, 320 pages
Publisher InTech
Published online 21, November, 2011
Published in print edition November, 2011

The book Radioisotopes - Applications in Bio-Medical Science contains two sections: Radioisotopes and Radiations in Bioscience and Radioisotopes and Radiology in Medical Science. Section I includes chapters on medical radioisotope production, radio-labeled nano-particles, radioisotopes and nano-medicine, use of radiations in insects, drug research, medical radioisotopes and use of radioisotopes in interdisciplinary fields etc. In Section II, chapters related to production of metal PET (positron emission tomography) radioisotopes, 3-dimensional and CT (computed tomography) scan, SS nuclear medicine in imaging, cancer diagnose and treatments have been included. The subject matter will by highly useful to the medical and paramedical staff in hospitals, as well as researchers and scholars in the field of nuclear medicine medical physics and nuclear bio-chemistry etc.

InTech Europe
University Campus STeP Ri
Slavka Krautzeka 83/A
51000 Rijeka, Croatia
Phone: +385 (51) 770 447
Fax: +385 (51) 686 166
www.intechopen.com

InTech China
Unit 405, Office Block, Hotel Equatorial Shanghai
No.65, Yan An Road (West), Shanghai, 200040, China
中国上海市延安西路65号上海国际贵都大饭店办公楼405单元
Phone: +86-21-62489820
Fax: +86-21-62489821

IntechOpen